

Electronic Supplementary Material (ESI)

## Coupling Thulium 4f Orbitals with Ni<sub>3</sub>Fe LDH to Form Electronic Buffer Band with Loaded Pt and Catalyzing Alkaline Overall Water Splitting

Xinping Yang,<sup>a</sup>, # Shucheng Li,<sup>a</sup>, # Yan Zhang,<sup>a</sup> Fagui Qiu,<sup>a</sup> Yanbin Sun,<sup>a</sup> Weikun Ning,<sup>a</sup> Qinglong Tao,<sup>b</sup> Wenqing Li,<sup>c</sup> and Shiding Miao <sup>a,\*</sup>

<sup>a</sup> Key Laboratory of Automobile Materials of Ministry of Education, School of Materials Science and Engineering, Solid Waste Recycling Engineering Research Centre of Jilin Province, Jilin University, Changchun, 130022, China;

<sup>b</sup> Zhejiang Taihua New Material Co., Ltd., Jiaxing, Zhejiang Prov., 314011, China;

<sup>c</sup> Key Laboratory of Mineral Resources Evaluation in Northeast Asia, Ministry of Natural Resources, Changchun 130061, China;

# Xinping Yang and Shucheng Li contributed equally to this work;

\* Corresponding author: E-mail: miaosd@iccas.ac.cn (S. Miao).

### Extra experimental details

#### Synthesis of Ni<sub>3</sub>Fe LDH

The amount of 3.0 mmol NiCl<sub>2</sub>·6H<sub>2</sub>O, 1.0 mmol FeCl<sub>3</sub>·6H<sub>2</sub>O were dissolved in 30.0 mL deionized water and stirred for 30 min, then the solutions was added by 20.0 mL aqueous solution containing 1.0 g C<sub>19</sub>H<sub>42</sub>BrN dropwise. Afterwards, the solution was homogeneously added by a fresh-prepared solution (20.0 mL) containing 200.0 mg NaBH<sub>4</sub> under stirring. For about 10.0 min the bubbles disappeared, and the solution

was further stirred for another 2.0 h. The precipitation was removed via centrifugation, and washed alternatively with deionized water and anhydrous ethanol for three runs. The sample was dried in vacuum at 60°C overnight to get Ni<sub>3</sub>Fe LDH powders.

#### *Synthesis of Ni<sub>3</sub>Fe LDH-Tm*

The preparative procedure of Ni<sub>3</sub>Fe LDH-Tm was similar to that of Ni<sub>3</sub>Fe LDH, except different moles of Tm(NO<sub>3</sub>)<sub>3</sub>·5H<sub>2</sub>O being added to the precursor solution. Samples obtained were named as the molar ratio of Tm to the sum of Ni and Fe. Samples were named Ni<sub>3</sub>Fe LDH-Tm0.01, Ni<sub>3</sub>Fe LDH-Tm0.03, Ni<sub>3</sub>Fe LDH-Tm0.05 and Ni<sub>3</sub>Fe LDH-Tm0.07, which means the content of Tm was 0.04 mmol, 0.12 mmol, 0.2 mmol and 0.28 mmol, respectively.

#### *Synthesis of Ni<sub>3</sub>Fe LDH-Tb*

Terbium at various concentrations were selected for control experiments, and the rest of experimental conditions were the same, except that, for example, 0.03 mmol of Tb(NO<sub>3</sub>)<sub>3</sub>·5H<sub>2</sub>O was replaced by 0.03 mmol Tb(NO<sub>3</sub>)<sub>3</sub>·5H<sub>2</sub>O. The amount of 3.0 mmol NiCl<sub>2</sub>·6H<sub>2</sub>O, 1.0 mmol FeCl<sub>3</sub>·6H<sub>2</sub>O were dissolved in the 30 mL deionized water and stirred for 30.0 min until clarified, and then 20.0 mL solution containing 1.0 g C<sub>19</sub>H<sub>42</sub>BrN was added dropwise under stirring. After the solution was homogeneous 200.0 mg NaBH<sub>4</sub> was add to the 20.0 mL solution. When the bubbles were disappeared, the solution was stirred for another 2.0 h. The sample was collected via centrifugation and washed three times with anhydrous ethanol and deionized water, respectively. The samples were dried in a vacuum oven at 60°C overnight and were named as Ni<sub>3</sub>Fe LDH-Tb. Similar procedures were used in preparing Yb-doped LDH

samples.

*Methods for electrochemical analyses*

All potentials to reversible hydrogen electrodes (RHE) were converted according to the following equation:

$$E_{RHE} = E_{Hg/HgO} + 0.098 + 0.059 \times PH \dots (S1)$$

The overpotentials were obtained as:

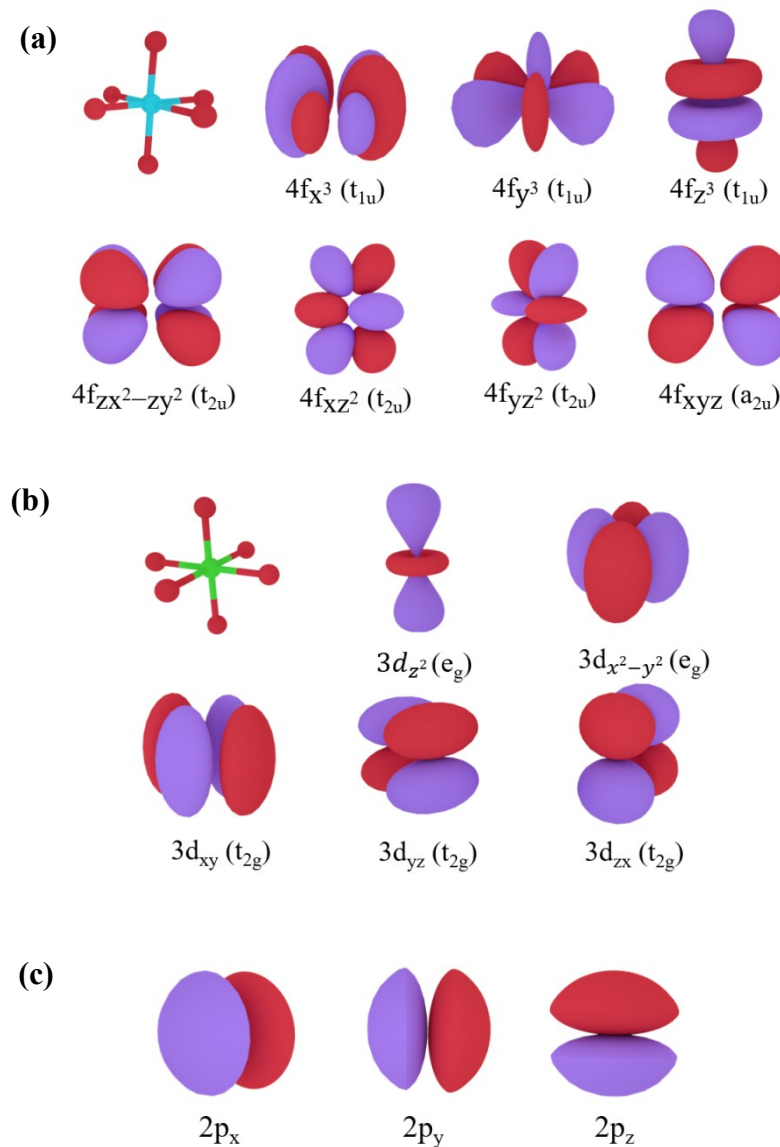
$$\eta_{OER} = E_{RHE} - 1.23 \dots (S2)$$

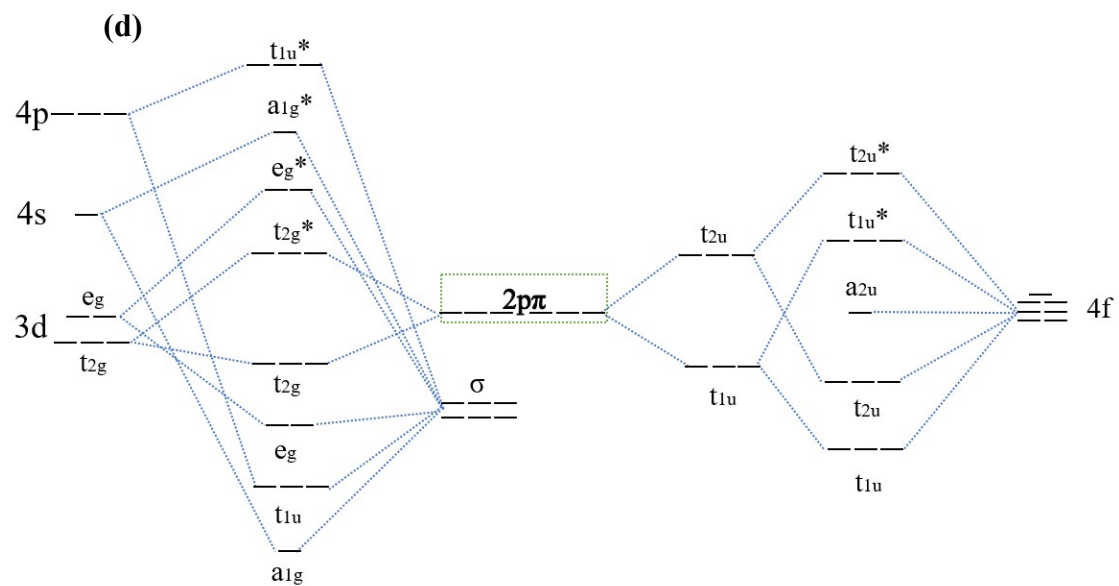
The formula for Tafel's slope, and the slop b was obtained as followed:

$$\eta = b \log j + a \dots (S3)$$

### Mott-Hubbard splitting

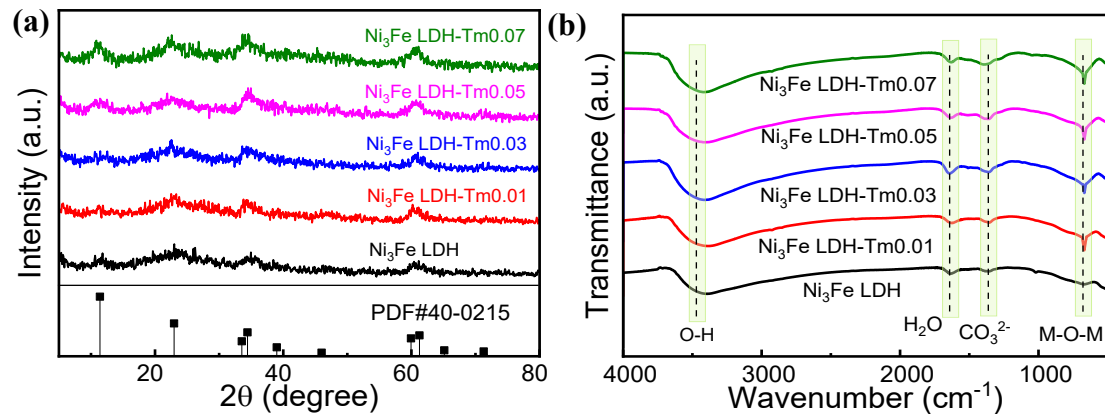
Based on Mott-Hubbard splitting, the orbital coupling of 4f, 3d, 2p orbitals of Tm were provided as follows showing the electronic configurations. The coordination of O atoms with Tm via sp-mixing orbitals to produce metal-oxygen (M-O) consisting with bonding of  $a_{1g}$ ,  $t_{1u}$ ,  $e_g$ , and  $t_{2g}$  and antibonding (M-O)\* of  $a_{1g}^*$ ,  $t_{1u}^*$ ,  $e_g^*$ , and  $t_{2g}^*$ . The configuration was listed as follows (Fig. S1).



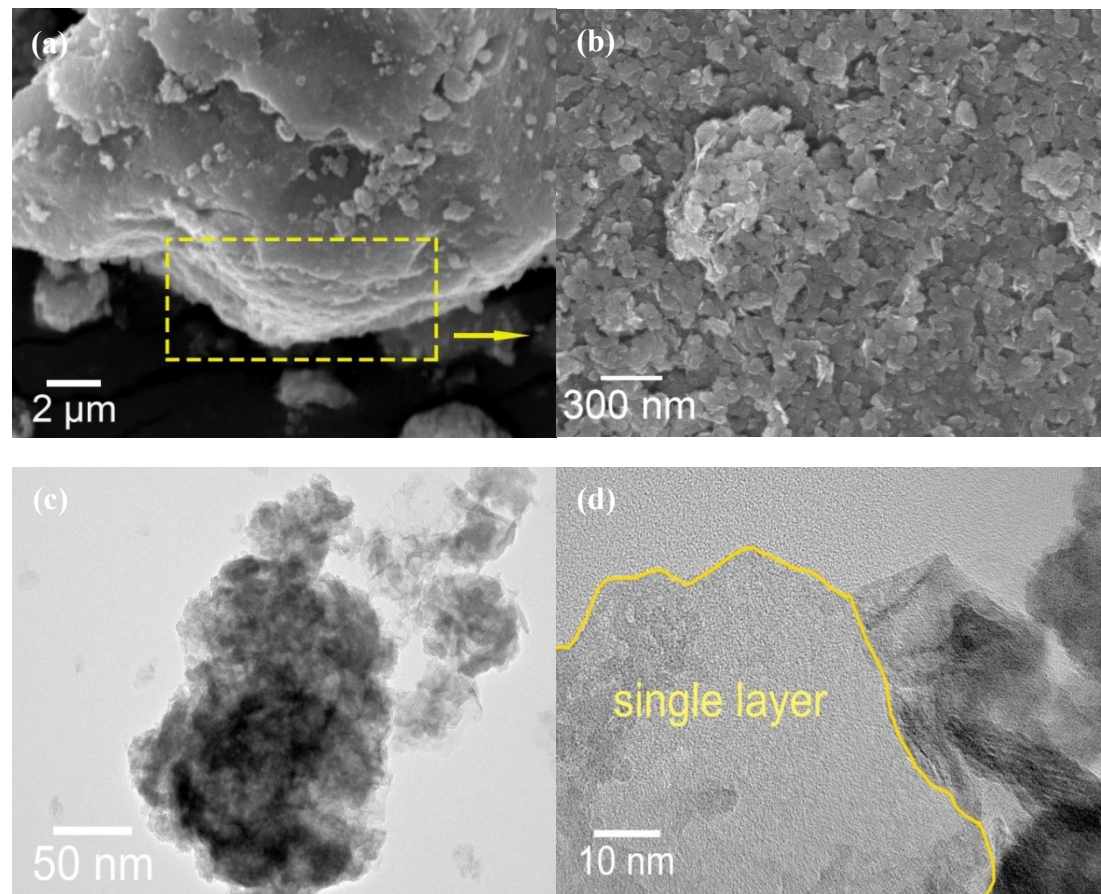


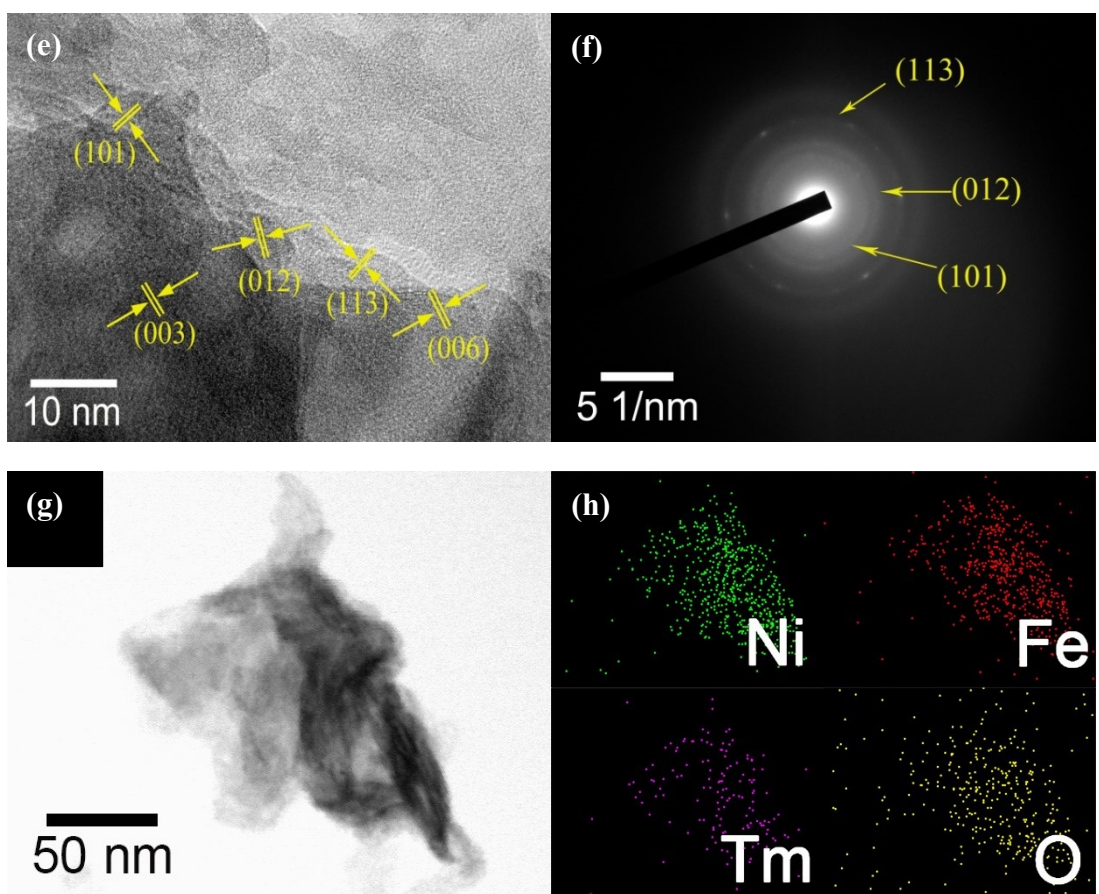
**Fig. S1** Orbital configuration diagram of (a) 4f orbital diagram; (b) 3d orbital diagram; and (c) 2p orbital diagram of O; (d) The qualitative molecular orbital diagram with an  $O_h$  symmetry.

*Series characterizations on Tm-doped samples including XRD, SEM, TEM, XPS, N<sub>2</sub> adsorption-desorption and electrochemical analyses (results shown as Fig. S2~Fig. S17, Table S1 and S2 provided OER performance and EIS parameters).*

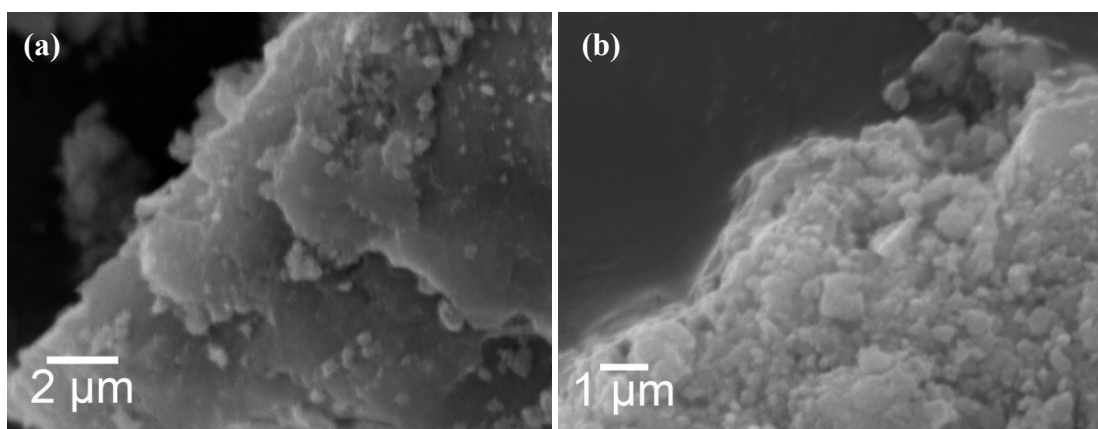


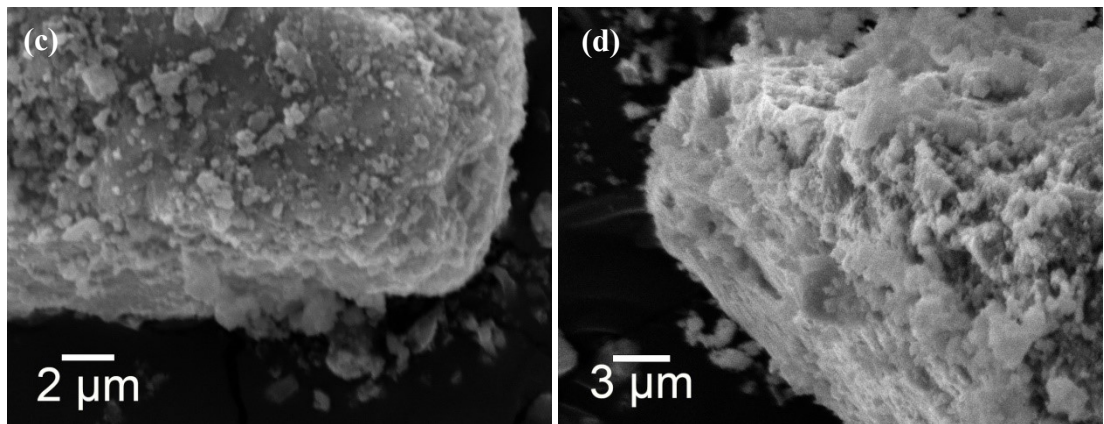
**Fig. S2** (a) XRD patterns and (b) FT-IR spectra of Ni<sub>3</sub>Fe LDH, Ni<sub>3</sub>Fe LDH-Tm0.01, Ni<sub>3</sub>Fe LDH-Tm0.03, Ni<sub>3</sub>Fe LDH-Tm0.05 and Ni<sub>3</sub>Fe LDH-Tm0.07.



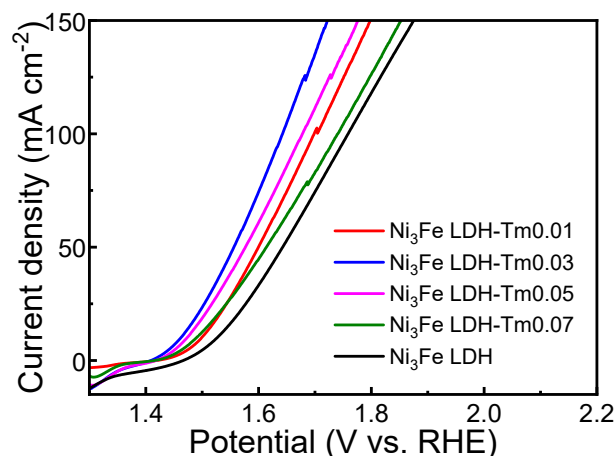


**Fig. S3** Morphological and structural characterizations on samples including: (a, b) SEM image, (c) TEM image, (d, e) HRTEM image with enlarged lattice structure, (f) SAED pattern and (g, h) corresponding EDS elemental mapping images of  $\text{Ni}_3\text{Fe}$  LDH-Tm0.03.

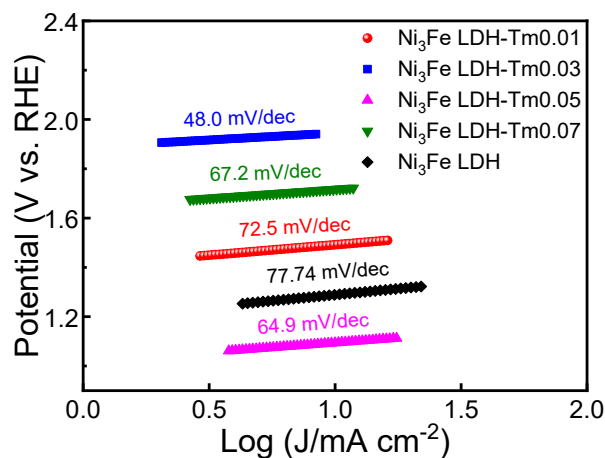




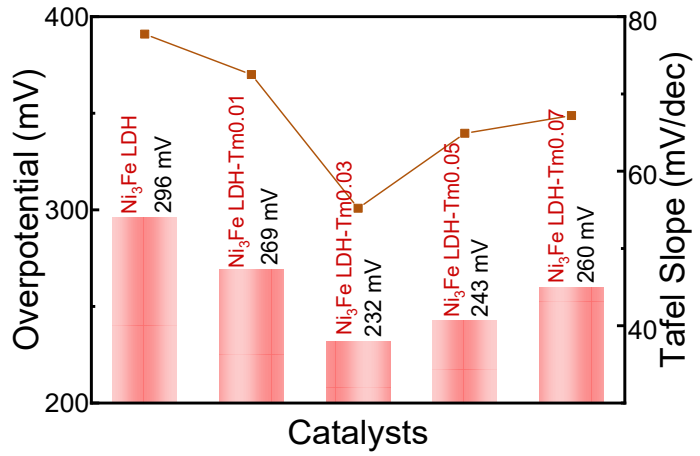
**Fig. S4** SEM image of (a)  $\text{Ni}_3\text{Fe}$  LDH, (b)  $\text{Ni}_3\text{Fe}$  LDH-Tm0.01, (c)  $\text{Ni}_3\text{Fe}$  LDH-Tm0.05 and (d)  $\text{Ni}_3\text{Fe}$  LDH-Tm0.07.



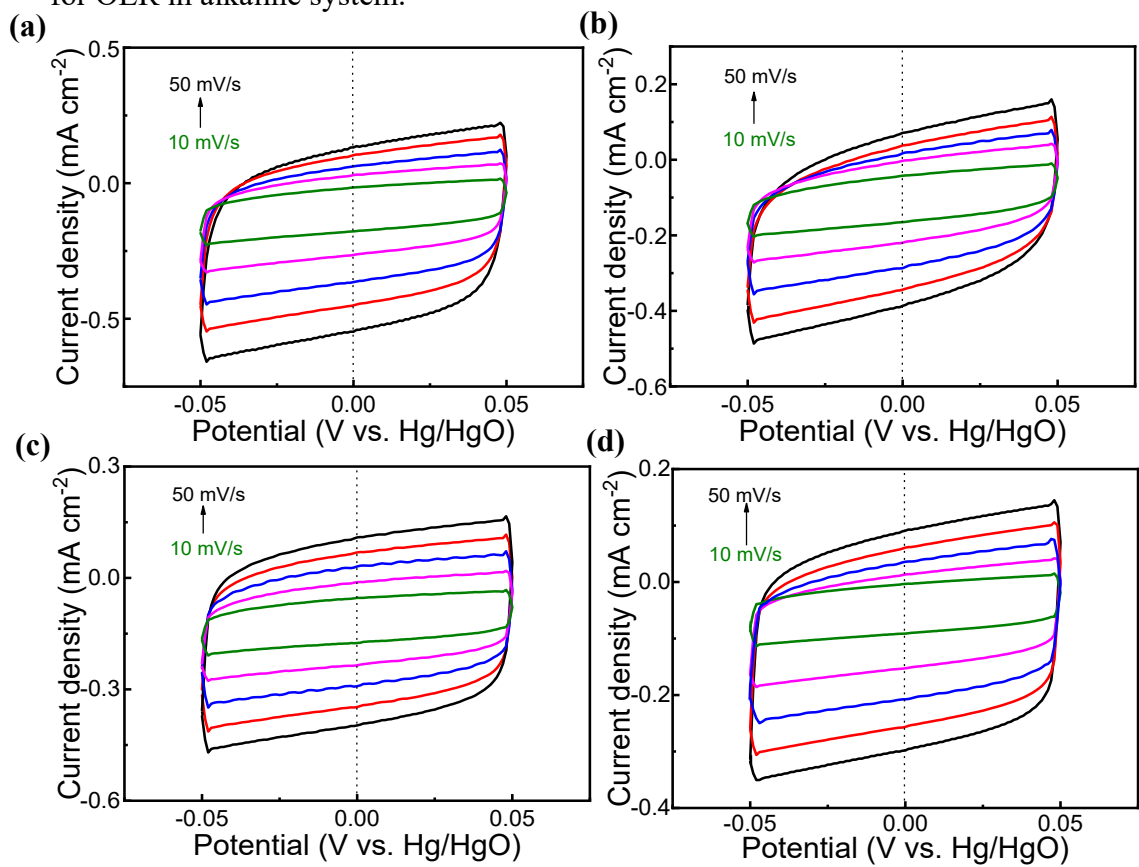
**Fig. S5** LSV curves of  $\text{Ni}_3\text{Fe}$  LDH,  $\text{Ni}_3\text{Fe}$  LDH-Tm0.01,  $\text{Ni}_3\text{Fe}$  LDH-Tm0.03,  $\text{Ni}_3\text{Fe}$  LDH-Tm0.05 and  $\text{Ni}_3\text{Fe}$  LDH-Tm0.07 conducted for OER in alkaline system.



**Fig. S6** Tafel curves of  $\text{Ni}_3\text{Fe}$  LDH,  $\text{Ni}_3\text{Fe}$  LDH-Tm0.01,  $\text{Ni}_3\text{Fe}$  LDH-Tm0.03,  $\text{Ni}_3\text{Fe}$  LDH-Tm0.05 and  $\text{Ni}_3\text{Fe}$  LDH-Tm0.07 conducted for OER in alkaline system.



**Fig. S7** Comparative diagram of the overpotential and Tafel slope values conducted for OER in alkaline system.



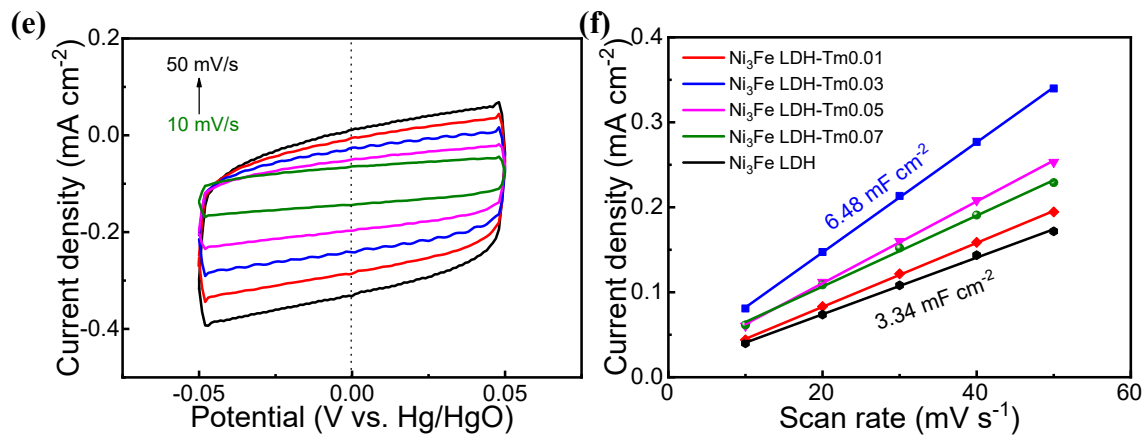


**Fig. S8** Cyclic voltammetry curves in the -0.05 V~0.05 V voltage range of (a) Ni<sub>3</sub>Fe LDH, (b) Ni<sub>3</sub>Fe LDH-Tm0.01, (c) Ni<sub>3</sub>Fe LDH-Tm0.03, (d) Ni<sub>3</sub>Fe LDH-Tm0.05 and (e) Ni<sub>3</sub>Fe LDH-Tm0.07 and (f) C<sub>dl</sub> values of different samples.

C<sub>dl</sub> was estimated by plotting the scan rates against current density (Fig. S8b):

$$C_{dl} = \frac{(j_a - j_c)}{2} \dots (S4)$$

while ECSA was calculated by the following equation:

$$ECSA = \frac{C_{dl}}{C_s} \dots (S5)$$

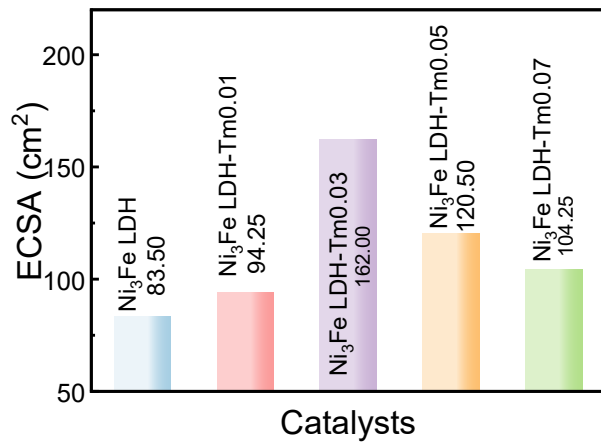


**Fig. S9** Comparison of ECSA values of different samples.

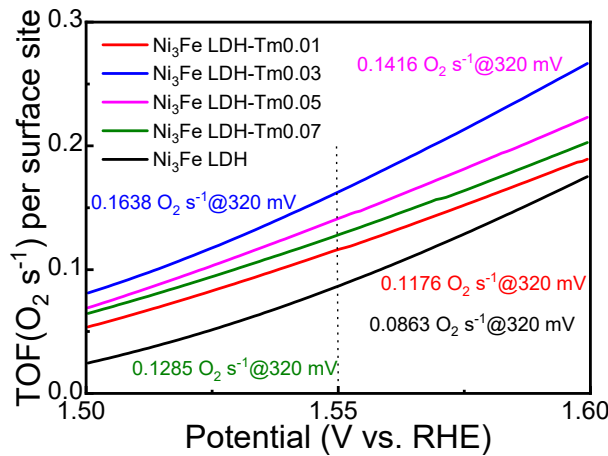


**Fig. S10** TOF curves of different samples conducted for OER in alkaline system.

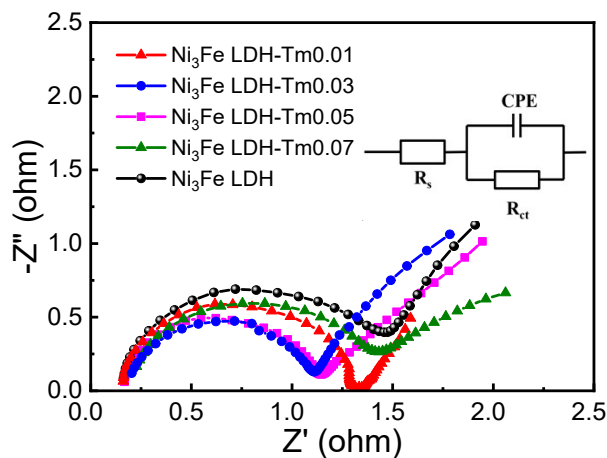


**Fig. S11** Nyquist plots of above samples (the equivalent circuit image was displayed in the inset) conducted for OER in alkaline system.

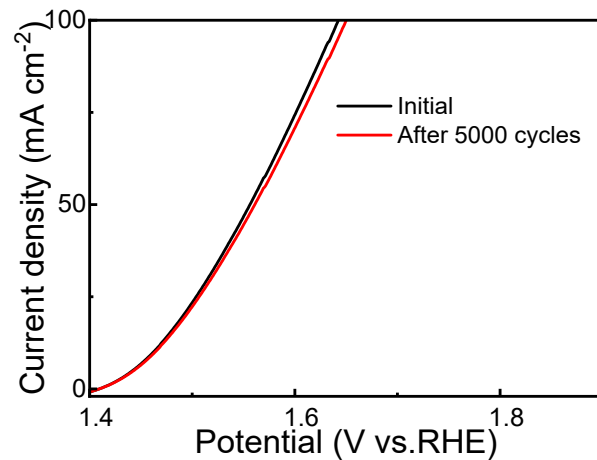


**Fig. S12** The polarization curves of Ni<sub>3</sub>Fe LDH-Tm0.03 before and after 5000 CV cycles in 1.0 M KOH solution.

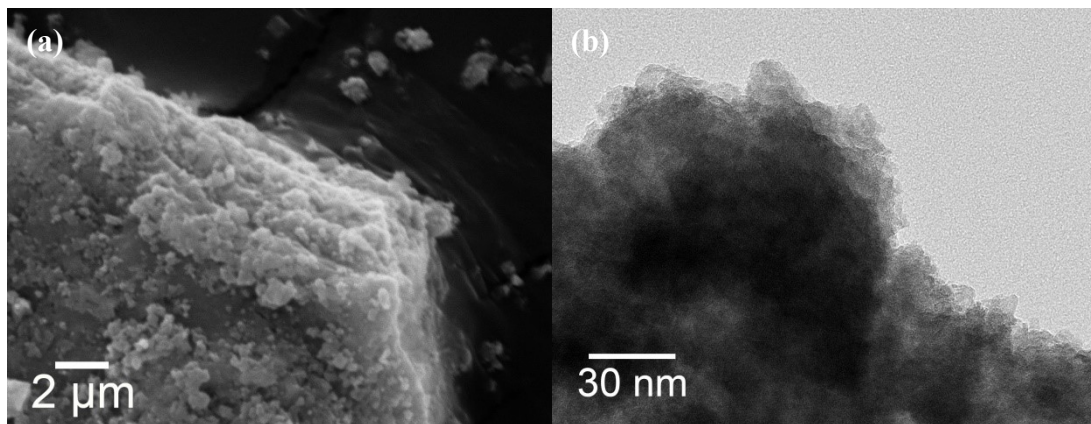


**Fig. S13** SEM image (a) and TEM image (b) of  $\text{Ni}_3\text{Fe}$  LDH-Tm after OER testing.

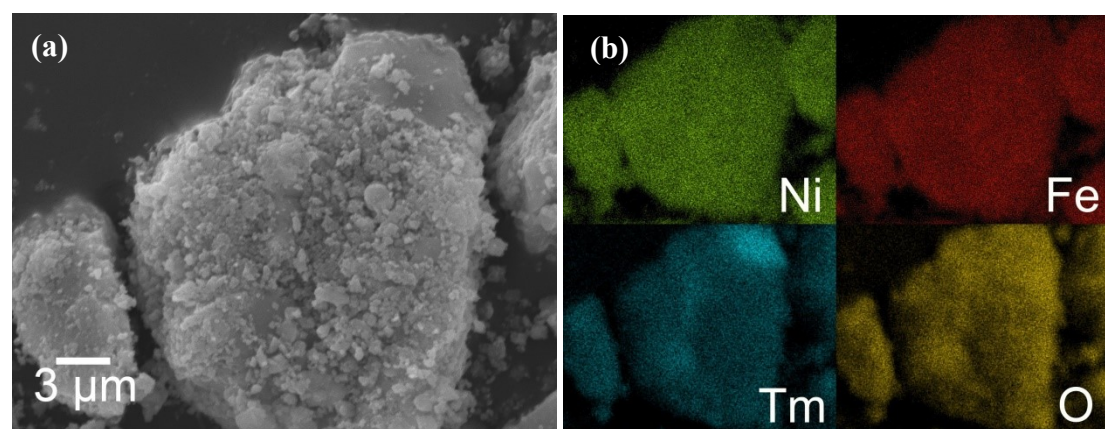


**Fig. S14** SEM image of  $\text{Ni}_3\text{Fe}$  LDH-Tm (a) and the corresponding EDS elemental mapping images (b) after OER testing.

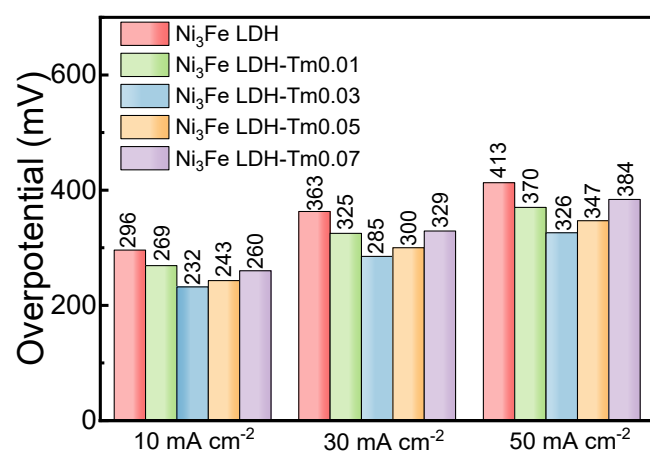


**Fig. S15** Comparison of overpotentials at different current densities.

Following formula was used to calculate the theoretical oxygen production:

$$n(O_2) = \frac{i \times t}{4 \times e \times N_A} \dots (S6)$$

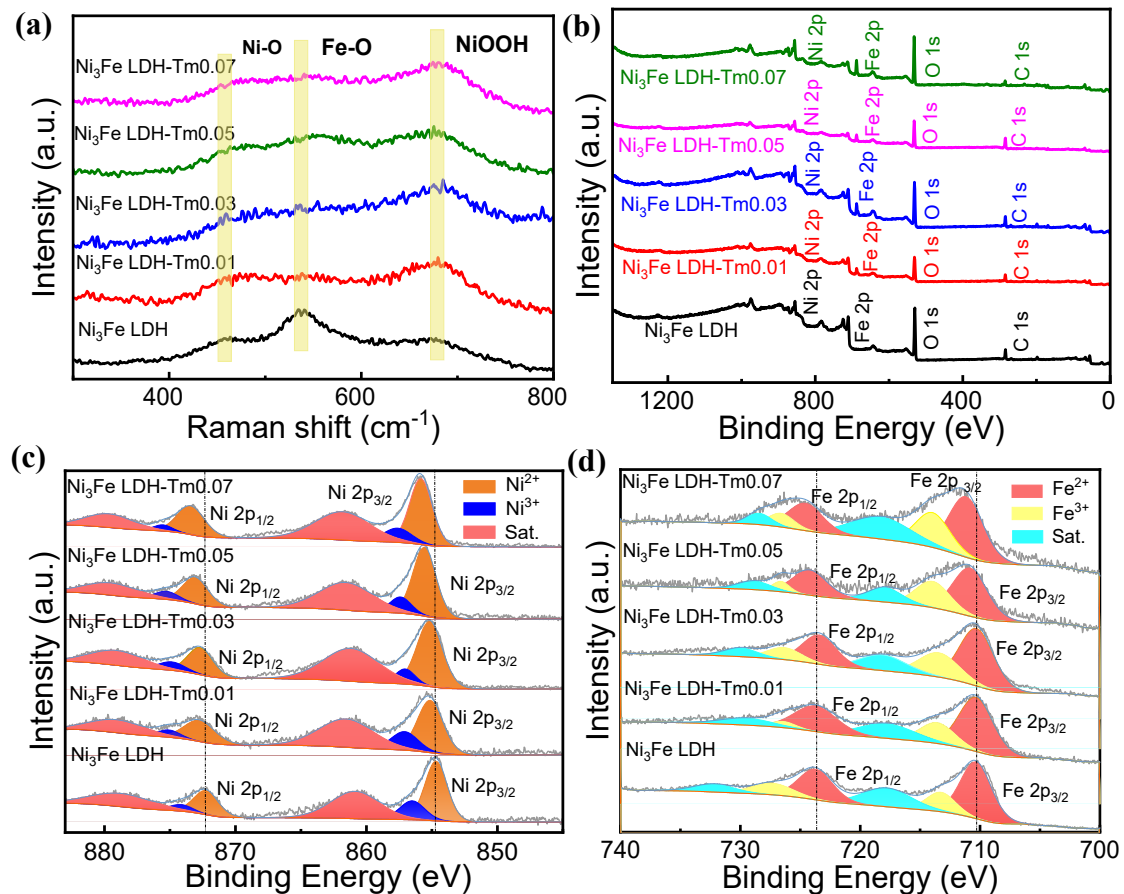
where the “i” is the current density,  $i=50$  mA cm $^{-2}$ , “t” is time and “e” is the elementary charge.

**Table S1** Comparison of OER performances of the as-prepared electrodes with that of other reported NiFe-based electrocatalysts evaluated.

Electrocatalyst	Electrolyte	Tafel slope (mV dec <sup>-1</sup> )	η/mV (at 10 mA cm <sup>-2</sup> )	Ref.
Ni <sub>3</sub> Fe LDH-Tm0.03	1 M KOH	48	230	This work
La-NiFe LDH	1 M KOH	77	340	<sup>1</sup>
NiFe-LDH Sn <sub>0.015</sub>	1 M KOH	66	250	<sup>2</sup>
LaNi <sub>1-x</sub> Fe <sub>x</sub> O <sub>3</sub>	1 M KOH	52	340	<sup>3</sup>
ZnO/NiFe-LDH	1 M KOH	67	320	<sup>4</sup>
NiFe LDH/C	0.1 M KOH	51	360	<sup>5</sup>
NiFe LDH-Bir	1 M KOH	55	260	<sup>6</sup>
NixFe <sub>3-x</sub> O <sub>4</sub>	1 M KOH	53	402	<sup>7</sup>
Ni-Fe-Ce-LDH	1 M KOH	54	246	<sup>8</sup>
Co <sup>2+</sup> /NiFe LDH	1 M KOH	59.4	264	<sup>9</sup>
S-NiFe-LDH/rGO	1 M KOH	55	265	<sup>10</sup>
Ru-NiFe LDH	1 M KOH	67.2	246	<sup>11</sup>
NiFe-LDH/Co-NC	1 M KOH	64	282	<sup>12</sup>
NiFeCo LDH	1 M KOH	57	270	<sup>13</sup>
NiFe-LDH@CNT	1 M KOH	51.4	255	<sup>14</sup>

**Table S2** EIS parameters of samples.

	R <sub>ct</sub>	CPE	R <sub>s</sub>
Ni <sub>3</sub> Fe LDH	2.446	0.001577	4.694
Ni <sub>3</sub> Fe LDH-Tm0.01	1.814	0.001099	2.987
Ni <sub>3</sub> Fe LDH-Tm0.03	0.9738	0.005289	0.854
Ni <sub>3</sub> Fe LDH-Tm0.05	1.06	0.003186	1.583
Ni <sub>3</sub> Fe LDH-Tm0.07	1.238	0.002495	1.846
Ni <sub>3</sub> Fe LDH-Tb	1.785	0.006579	3.853
Ni <sub>3</sub> Fe LDH-Yb	1.699	0.001891	4.024



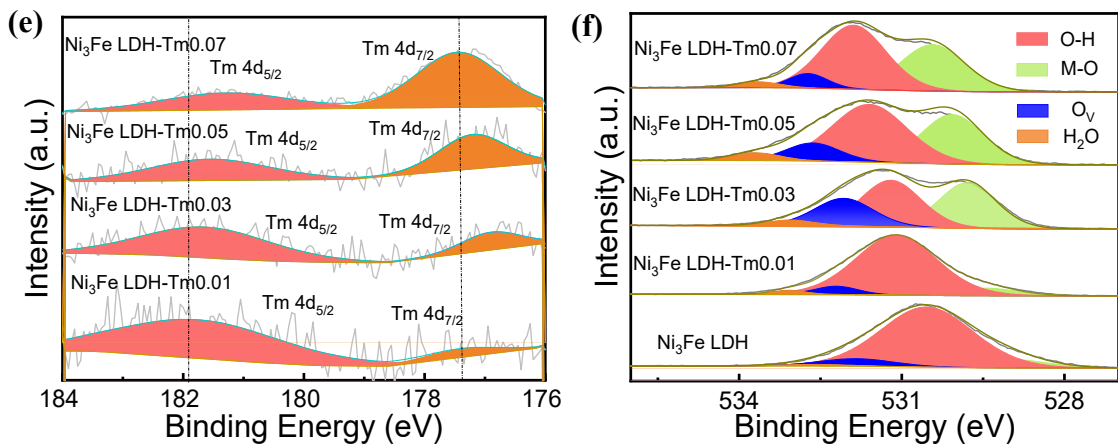


**Fig. S16** (a) Raman spectra, (b) XPS survey spectra of the samples and High resolution: (c) Ni 2p, (d) Fe 2p, (e) Tm 4d and (f) O 1s.

The percentage of Ni<sup>3+</sup> was calculated by the following equation:

$$C_{(Ni^{3+})} = \frac{Area(Ni^{3+})}{Area(Ni^{2+}) + Area(Ni^{3+})} \times 100\% \dots (S7)$$

The optical band gap of all samples is determined by using the equation:

$$(\alpha h\nu)^n = k(h\nu - E_g) \dots (S8)$$

$$h\nu = \frac{1240}{Wavelength} \dots (S9)$$

$$(\alpha h\nu)^n = (2.303 \times Absorbance \times Energy)^n \dots (S10)$$

where  $\alpha$  is the absorbance coefficient and n=2 for direct transition and n=0.5 for indirect transition.

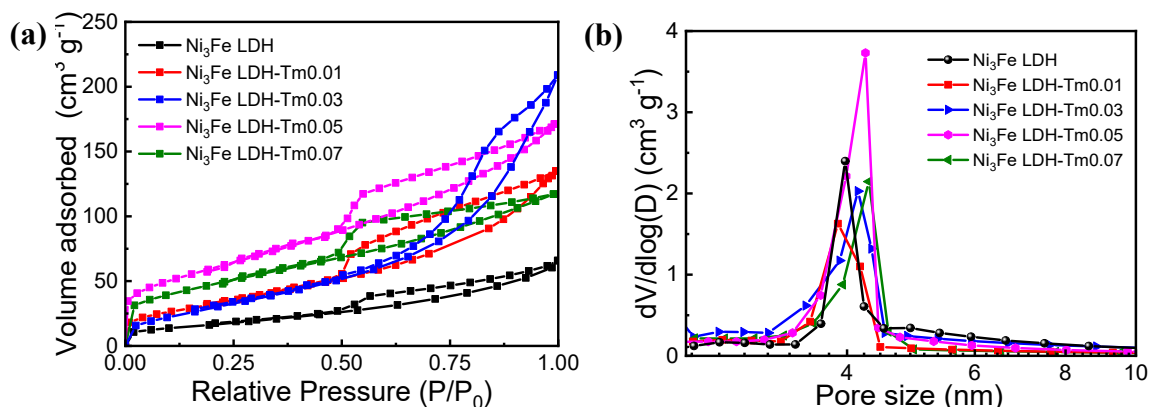


**Fig. S17** (a) Nitrogen adsorption-desorption isotherms and (b) BJH pore size

distribution curves of the samples.

*Series characterizations on REE ( $Tm$ ,  $Tb$ , and  $Yb$ )-doped samples for comparison study, which included the XRD, SEM, TEM, XPS, electrochemical analyses, contact angle measurements, and  $N_2$  adsorption-desorption isotherms (Fig. S18~Fig. S36).*

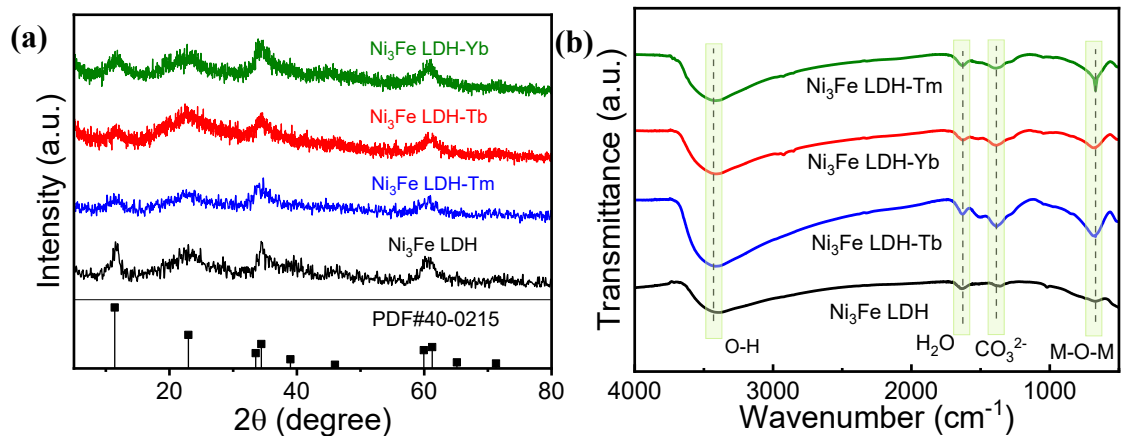


**Fig. S18** (a) XRD patterns and (b) FT-IR spectra of  $\text{Ni}_3\text{Fe LDH}$ ,  $\text{Ni}_3\text{Fe LDH-Tb}$ ,  $\text{Ni}_3\text{Fe LDH-Tm}$  and  $\text{Ni}_3\text{Fe LDH-Yb}$ .

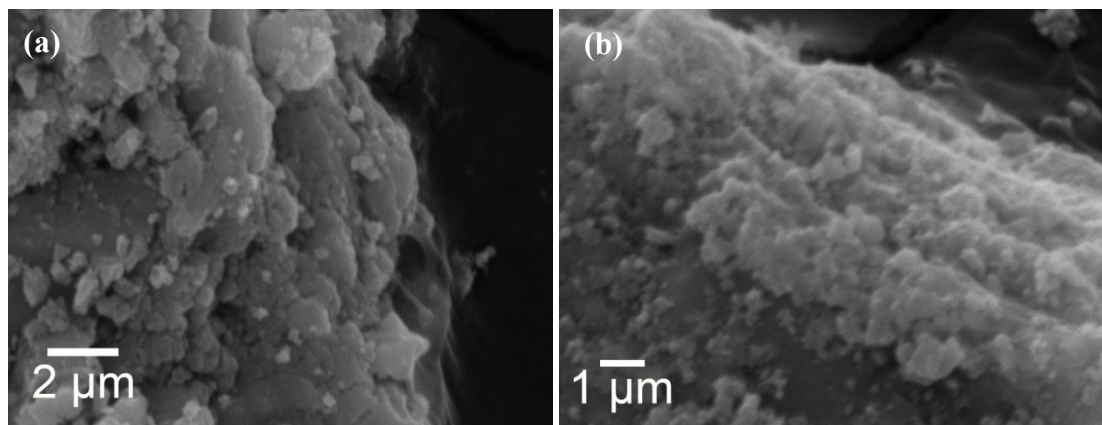


**Fig. S19** SEM image of (a)  $\text{Ni}_3\text{Fe LDH-Tb}$  and (b)  $\text{Ni}_3\text{Fe LDH-Yb}$ .

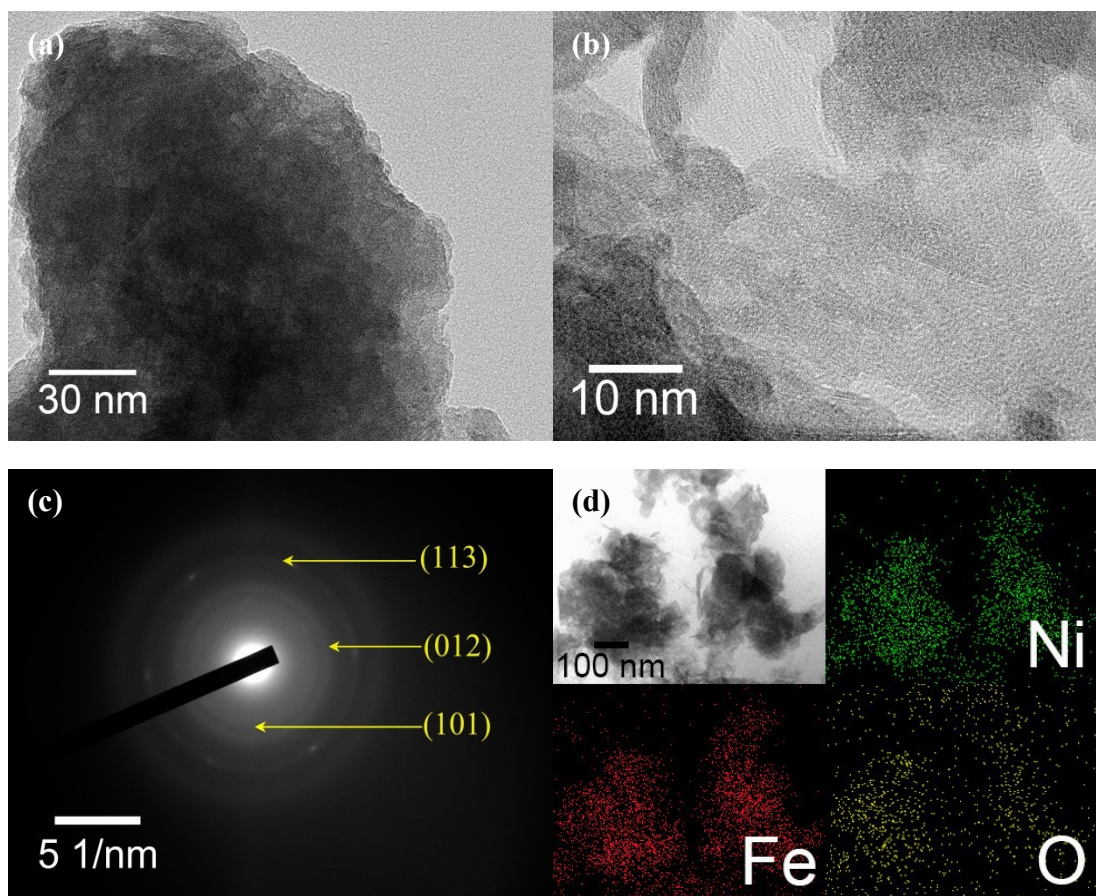


**Fig. S20** (a) TEM, (b) HRTEM image, (c) SAED pattern and (d) EDS elemental mapping images of  $\text{Ni}_3\text{Fe}$  LDH.

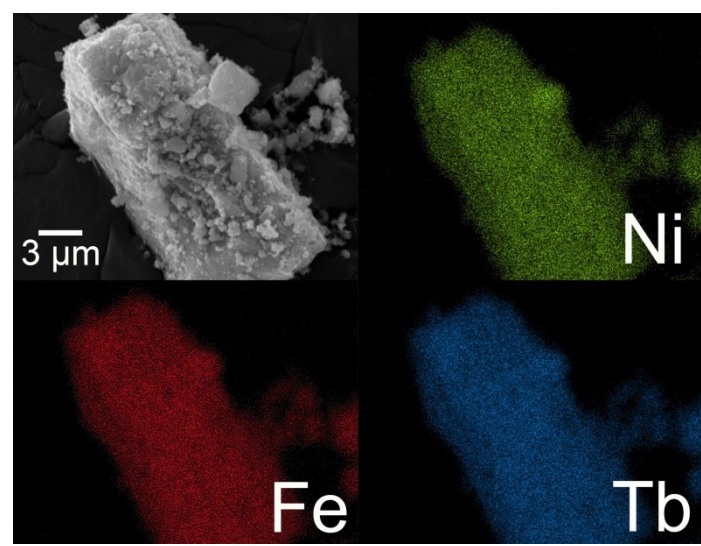


**Fig. S21** EDS elemental mapping images of  $\text{Ni}_3\text{Fe}$  LDH-Tb.

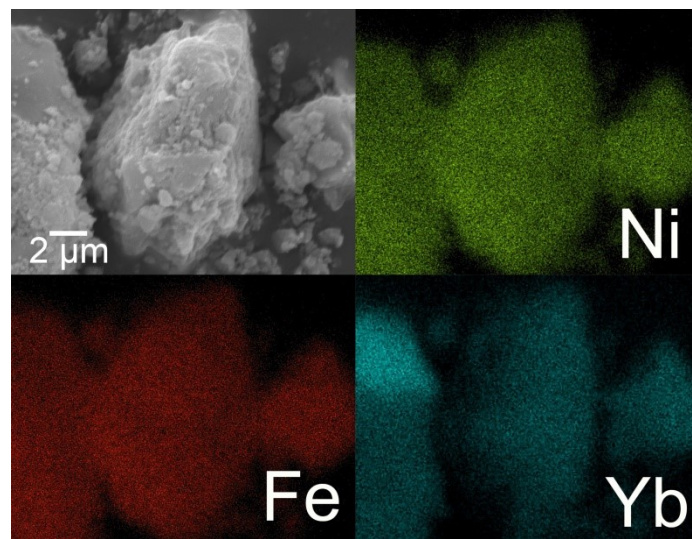


**Fig. S22** EDS elemental mapping images of  $\text{Ni}_3\text{Fe}$  LDH-Yb.

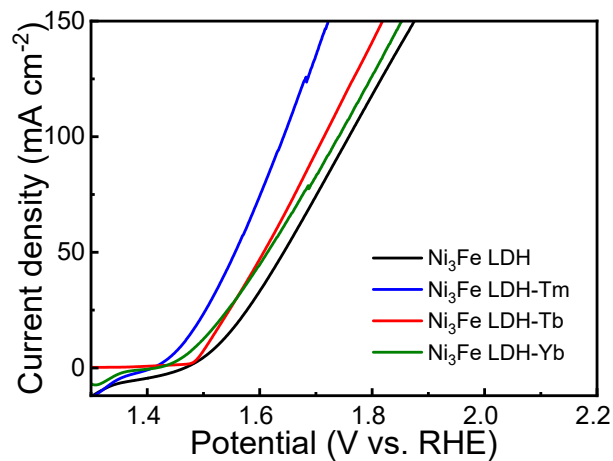


**Fig. S23** LSV curves of  $\text{Ni}_3\text{Fe}$  LDH,  $\text{Ni}_3\text{Fe}$  LDH-Tb,  $\text{Ni}_3\text{Fe}$  LDH-Tm and  $\text{Ni}_3\text{Fe}$  LDH-Yb for OER.

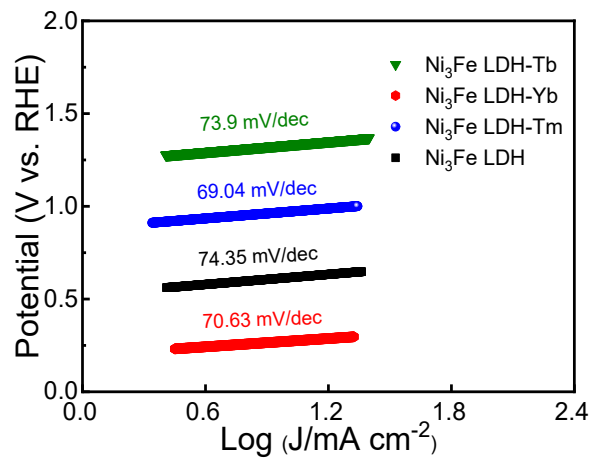


**Fig. S24** Tafel plots of  $\text{Ni}_3\text{Fe}$  LDH,  $\text{Ni}_3\text{Fe}$  LDH-Tb,  $\text{Ni}_3\text{Fe}$  LDH-Tm and  $\text{Ni}_3\text{Fe}$  LDH-Yb.

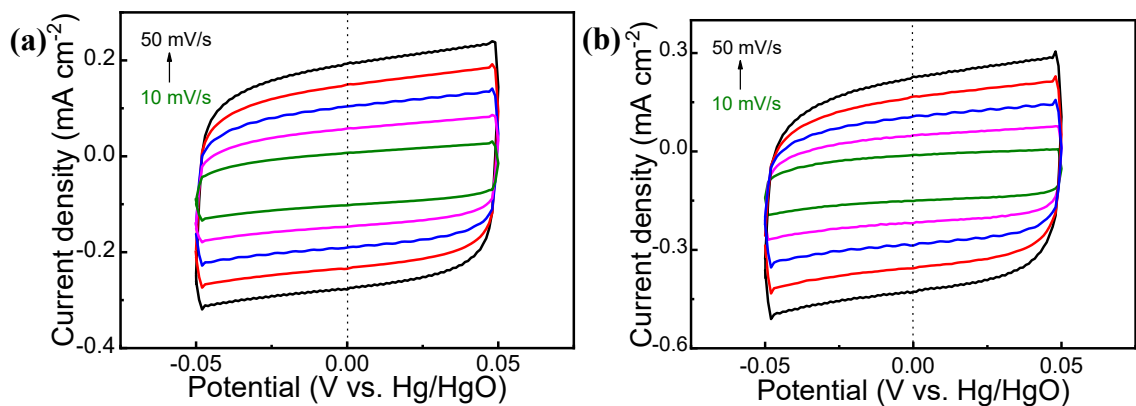


**Fig. S25** Cyclic voltammetry curves in the -0.05 V~0.05 V voltage range of (a) Ni<sub>3</sub>Fe LDH-Tb and (b) Ni<sub>3</sub>Fe LDH-Yb.

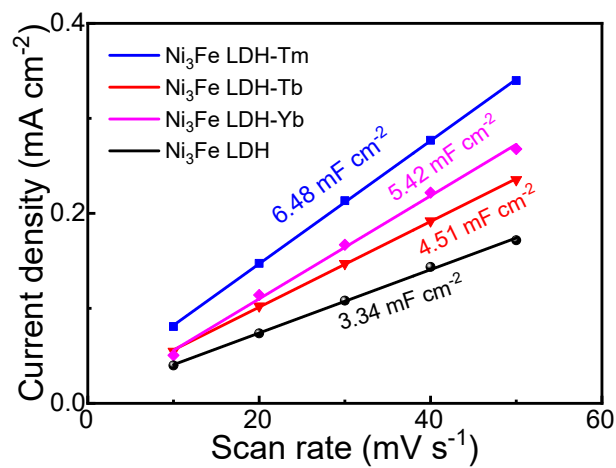


**Fig. S26** C<sub>dl</sub> values of different samples.

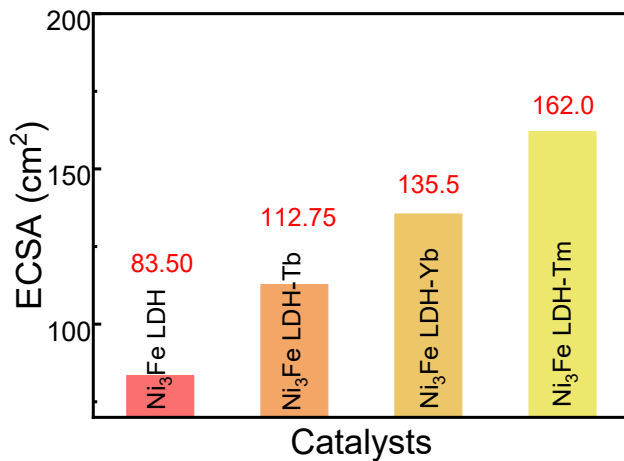


**Fig. S27** Comparison of ECSA values of different samples.

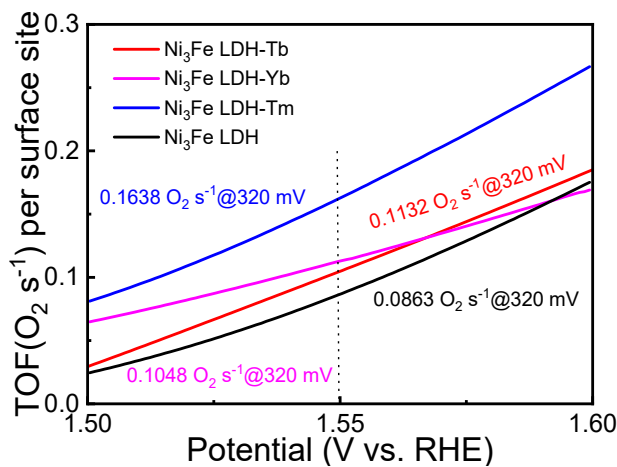
$$TOF_{per\ site} = \frac{total\ hydrogen\ turnover/cm^2\ geometric\ area}{surface\ sites\ of\ catalyst/cm^2\ geometric\ area} \dots (S11)$$

$$\begin{aligned} & total\ hydrogen\ turnover/cm^2\ geometric\ area\ (OER) \\ &= \frac{6.02 \times 10^{23}}{1\ mol\ O_2} \times \frac{1\ mol\ O_2}{4\ mol\ e^-} \times \frac{1\ mol\ e^-}{96485\ C} \times \frac{1\ C\ s^{-1}}{1000\ mA} \times j_{OER} \frac{mA}{cm^2} \end{aligned}$$

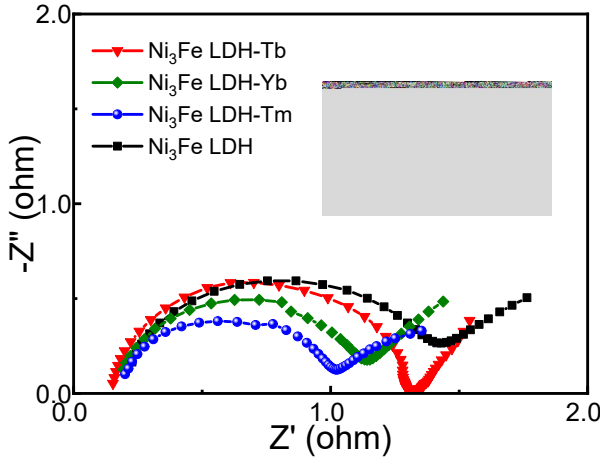
$$\begin{aligned} & surface\ sites\ of\ catalyst/cm^2\ geometric\ area \\ &= ECSA \times \frac{total\ number\ of\ atoms}{cm^2\ unit\ cell} \end{aligned}$$

Lattice parameters:  $a=b=3.079\ \text{\AA}$ ,  $c=22.790\ \text{\AA}$ ,  $\alpha=\beta=90^\circ$ ,  $\gamma=120^\circ$ . Volume of the hexagonal cell =  $187.11\ \text{\AA}^3$ .

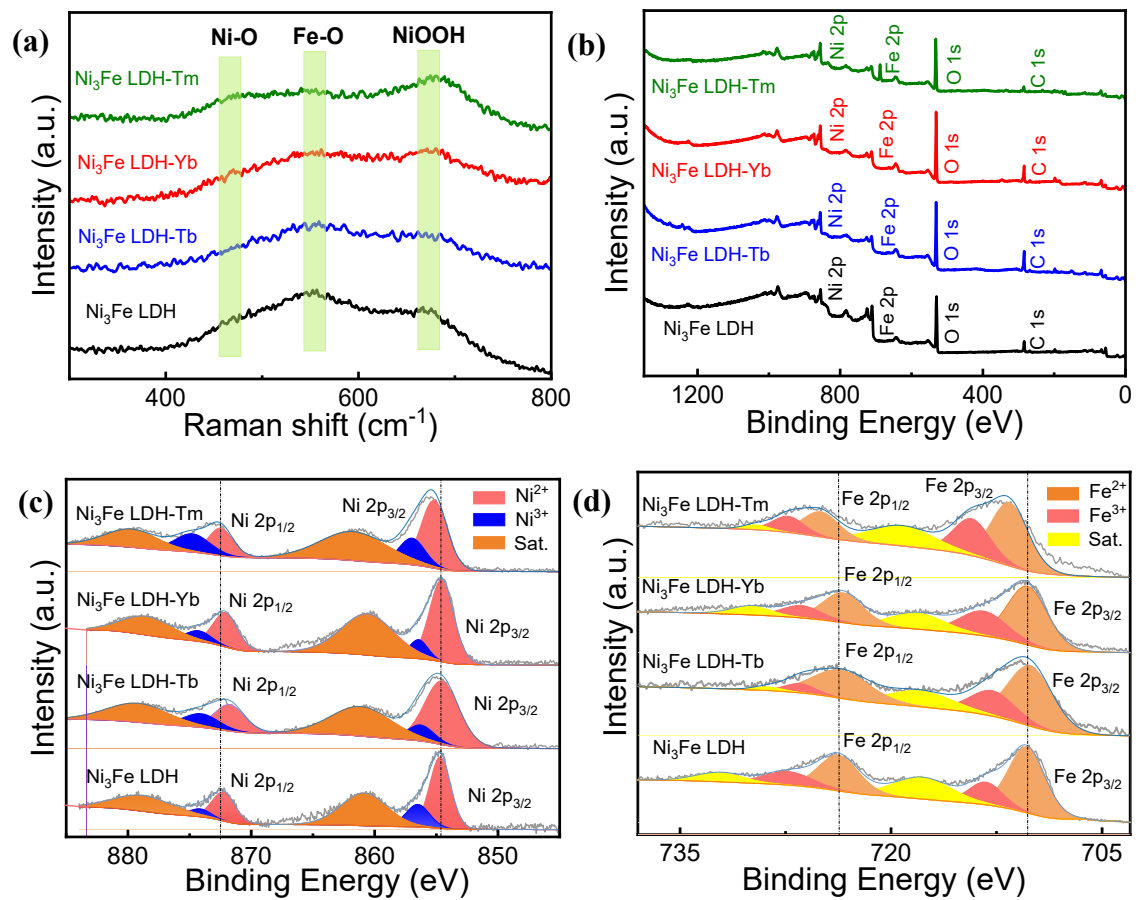
$$\begin{aligned} & surface\ sites\ of\ catalyst/cm^2\ geometric\ area \\ &= ECSA \times \left( \frac{39\ atoms\ per\ unit\ cell}{187.11\ \text{\AA}^3} \right)^2 \end{aligned}$$



**Fig. S28** TOF curves of different samples.



**Fig. S29** Nyquist plots of above samples (the equivalent circuit image is displayed in the inset).



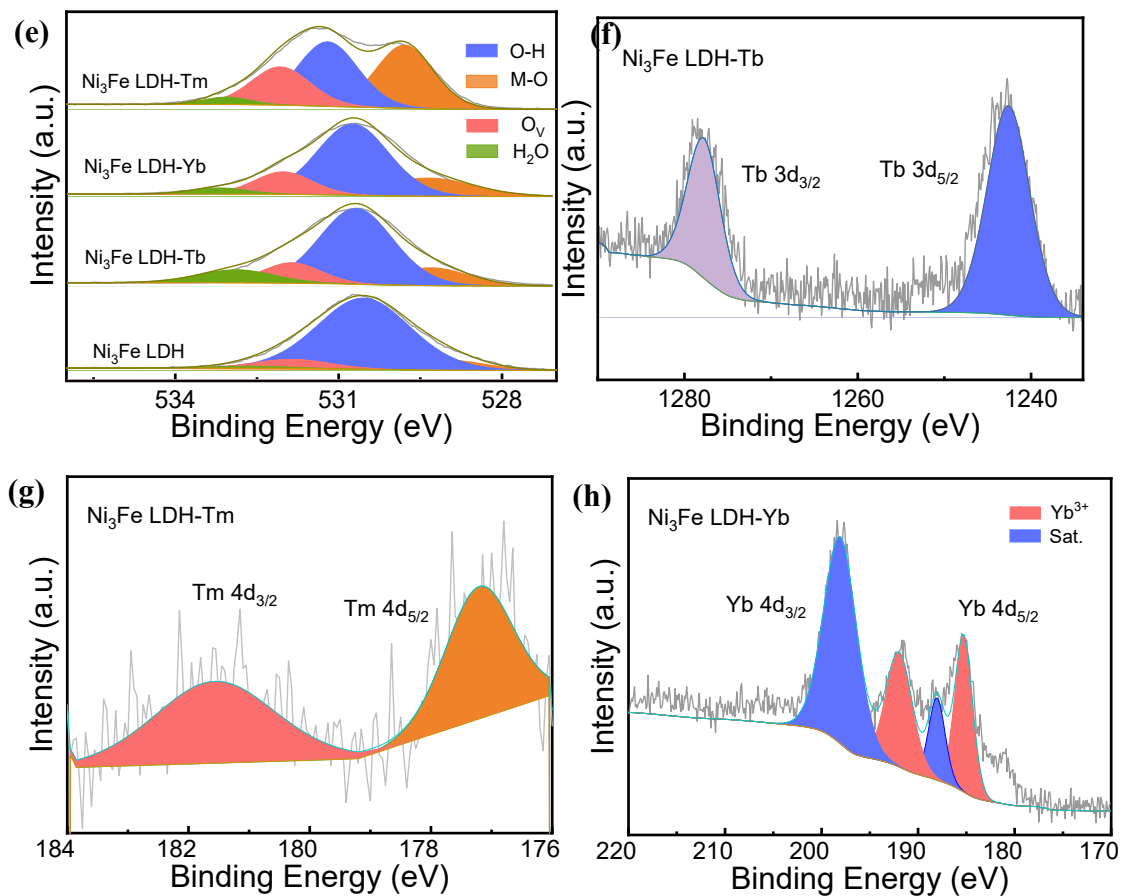


**Fig. S30** (a) Raman spectra, (b) XPS survey spectra of the samples and high resolution: (c) Ni 2p, (d) Fe 2p, (e) O 1s, (f) Tb 3d, (g) Tm 4d and (h) Yb 4d.

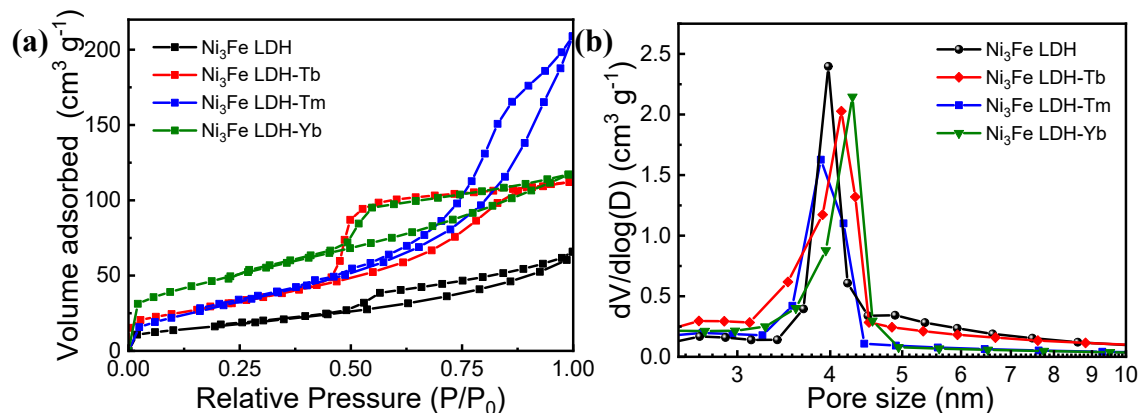


**Fig. S31** (a) Nitrogen adsorption-desorption isotherms and (b) BJH pore size distribution curves of the samples.

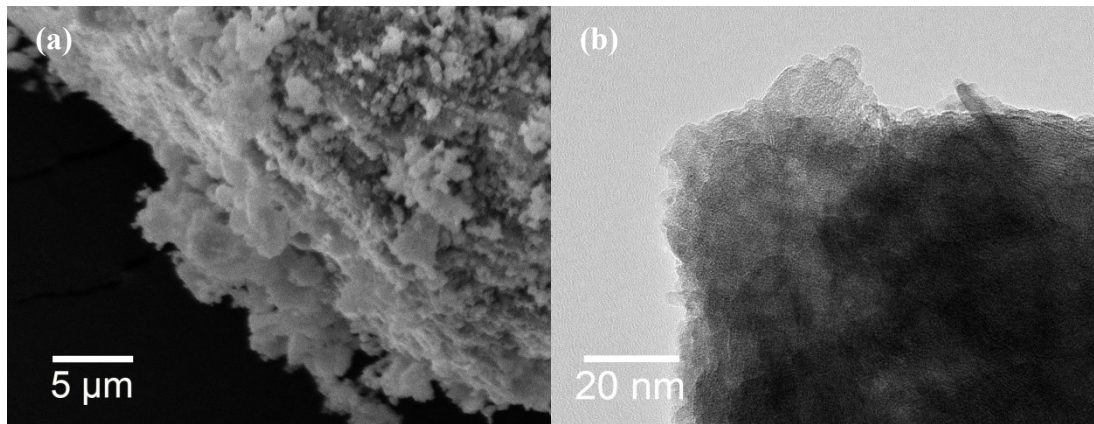


**Fig. S32** (a) SEM image and (b) TEM image of  $\text{Ni}_3\text{Fe}$  LDH/ $\text{NiFe}_2\text{O}_4$ /Pt.

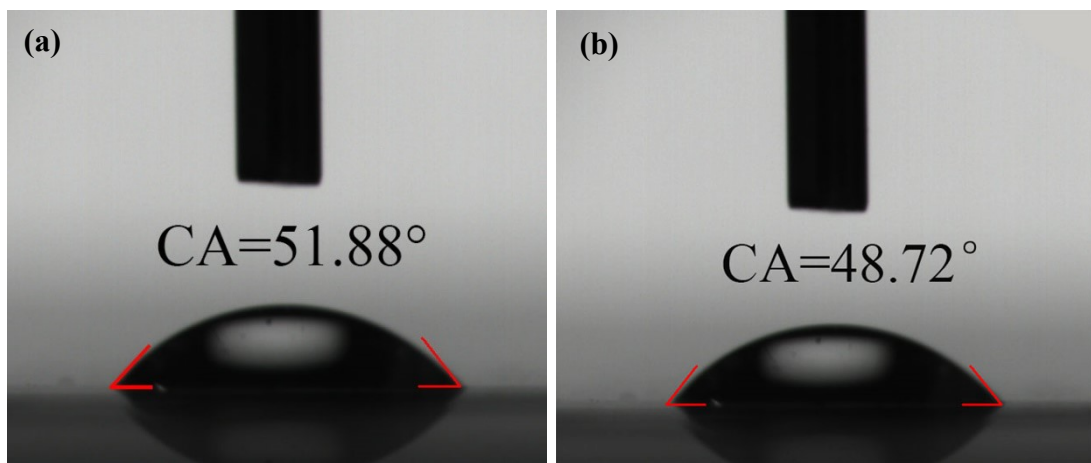


**Fig. S33** The contact angle of  $\text{Ni}_3\text{Fe}$  LDH and  $\text{Ni}_3\text{Fe}$  LDH/ $\text{NiFe}_2\text{O}_4$ /Pt-Tm.

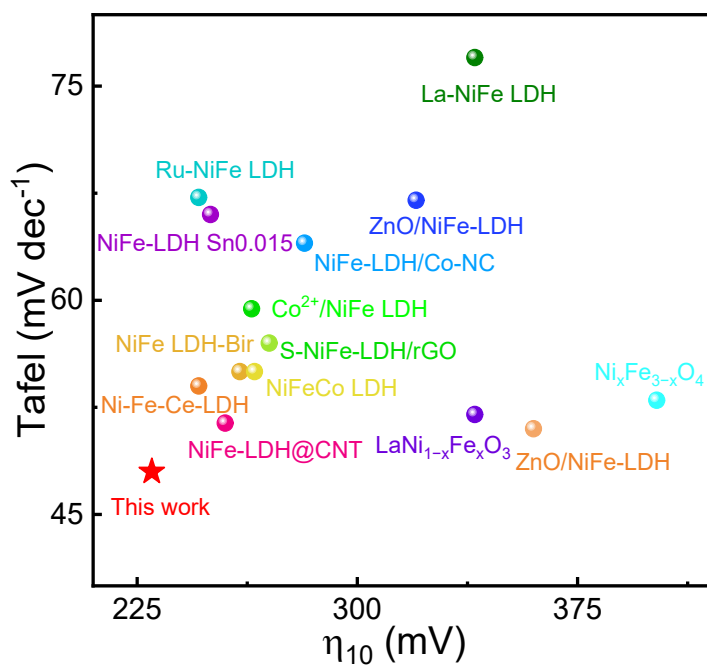


**Fig. S34** Comparison of the overpotentials and Tafel plots for various NiFe-based

catalysts reported.

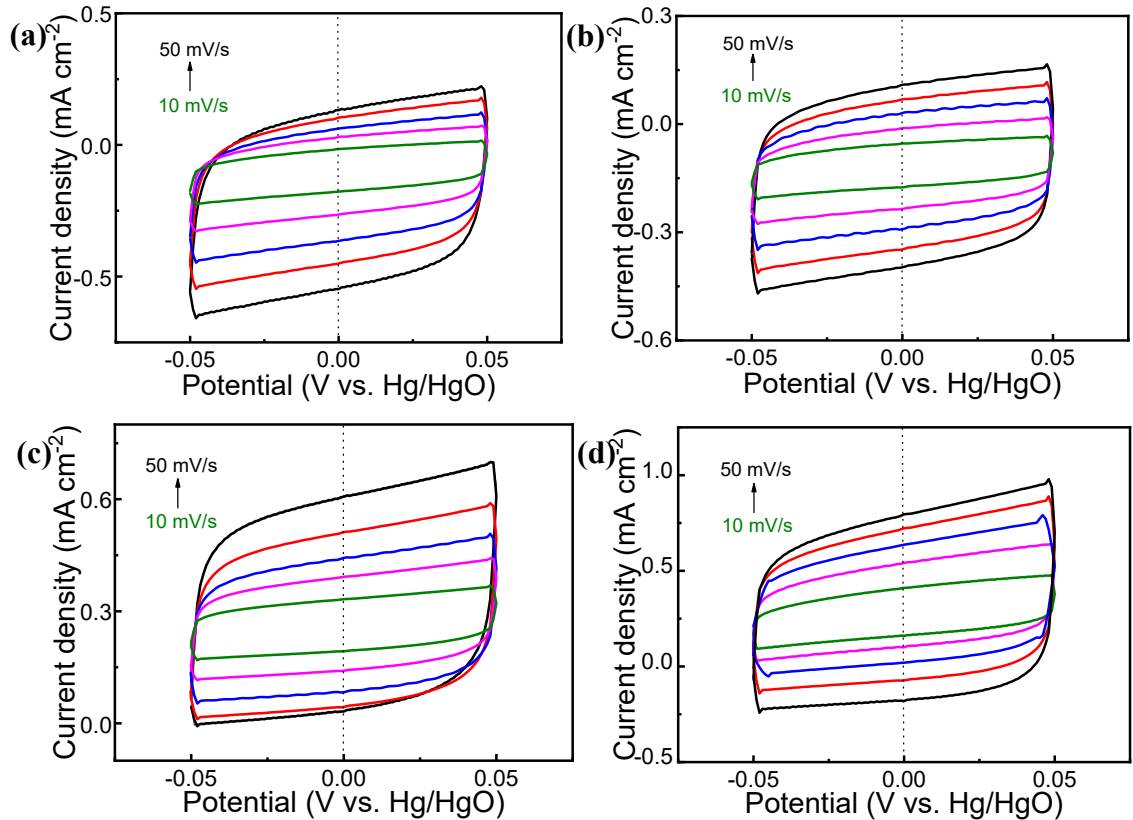


**Fig. S35** Cyclic voltammetry curves in the -0.05 V~0.05 V voltage range of (a)  $\text{Ni}_3\text{Fe}$  LDH, (b)  $\text{Ni}_3\text{Fe}$  LDH-Tm, (c)  $\text{Ni}_3\text{Fe}$  LDH/ $\text{NiFe}_2\text{O}_4$ /Pt and (d)  $\text{Ni}_3\text{Fe}$  LDH/ $\text{NiFe}_2\text{O}_4$ /Pt-Tm.

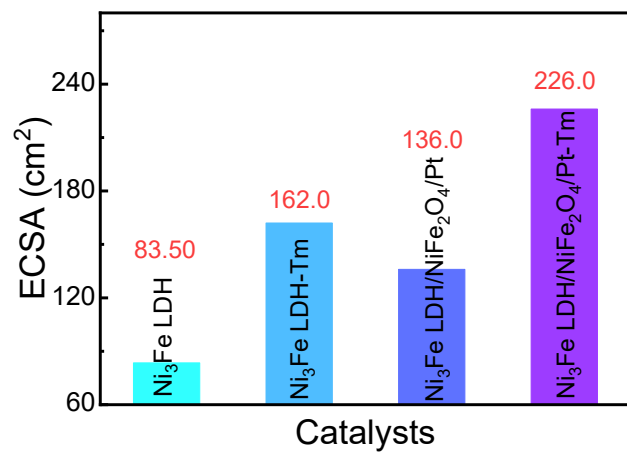


**Fig. S36** Comparison of ECSA values of different samples.

*Electrochemical measurements on overall water splitting catalyzed by the Ni<sub>3</sub>Fe LDH/NiFe<sub>2</sub>O<sub>4</sub>/Pt-Tm (Fig. S37~Fig. S41, and Table S3 provided comparison with reported data on OER and HER performances)*

$$TOF_{per\ site} = \frac{total\ hydrogen\ turnover/cm^2\ geometric\ area}{surface\ sites\ of\ catalyst/cm^2\ geometric\ area} \dots (S12)$$

$$\begin{aligned} & total\ hydrogen\ turnover/cm^2\ geometric\ area\ (HER) \\ &= \frac{6.02 \times 10^{23}}{1\ mol\ H_2} \times \frac{1\ mol\ H_2}{2\ mol\ e^-} \times \frac{1\ mol\ e^-}{96485\ C} \times \frac{1\ C\ s^{-1}}{1000\ mA} \times |j_{HER}| \frac{mA}{cm^2} \end{aligned}$$

$$\begin{aligned} & surface\ sites\ of\ catalyst/cm^2\ geometric\ area \\ &= ECSA \times \frac{total\ number\ of\ atoms}{cm^2\ unit\ cell} \end{aligned}$$

Lattice parameters: a=b=3.079 Å, c=22.790 Å, α=β=90°, γ=120°. Volume of the hexagonal cell = 187.11 Å<sup>3</sup>.

$$\begin{aligned} & surface\ sites\ of\ catalyst/cm^2\ geometric\ area \\ &= ECSA \times \left( \frac{39\ atoms\ per\ unit\ cell}{187.11\text{\AA}^3} \right)^2 \end{aligned}$$

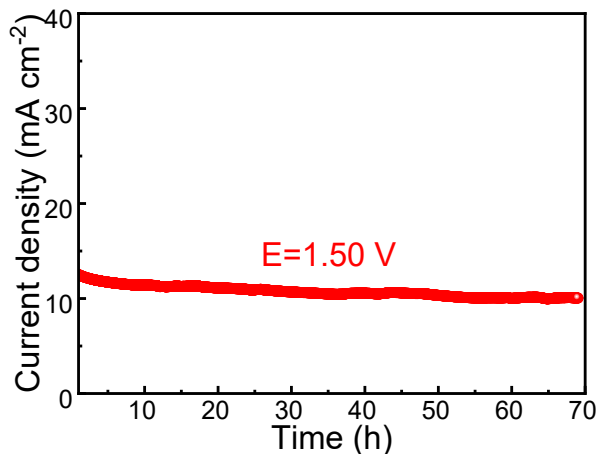


**Fig. S37** Chronoamperometric response at a constant overpotential of 1.50 V.

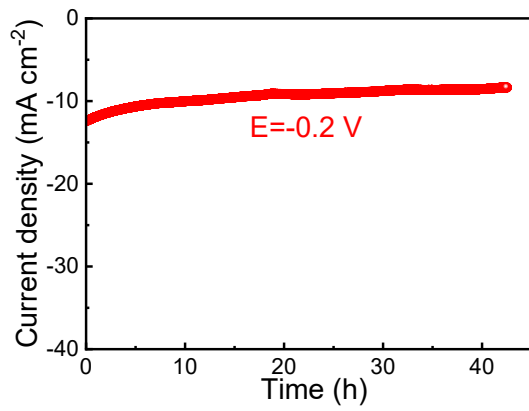


**Fig. S38** Chronoamperometric response at a constant overpotential of  $-0.2 \text{ V}$ .

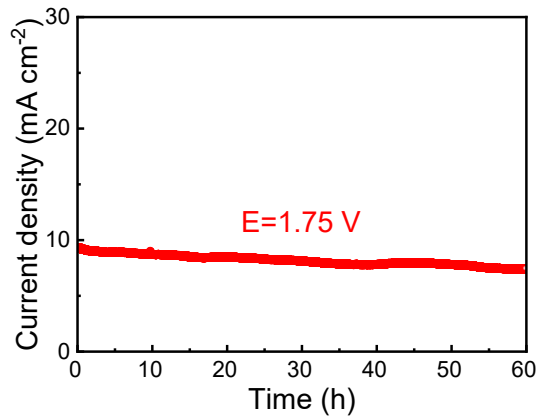


**Fig. S39** Chronoamperometric response at a constant overpotential of  $1.75 \text{ V}$ .



**Fig. S40** The Hoffmann electrolytic device for overall water splitting.

We calculated the energy efficiency of overall water electrolysis at the current density of  $10 \text{ mA cm}^{-2}$  as follows. The specific energy for producing  $1.0 \text{ kg}$  of hydrogen is thermodynamically given as  $143 \text{ MJ kg}^{-1}$  or  $39.4 \text{ kWh kg}^{-1}$ . Since the

electrolysis cell operates near 1.690 V at 10 mA cm<sup>-2</sup>, the energy required for producing 1.0 kg H<sub>2</sub> can be calculated as follows. The current density of 10 mA cm<sup>-2</sup> can be expressed as 0.01 C s<sup>-1</sup> cm<sup>-2</sup> ( $\because 1\text{ A} = 1\text{ C s}^{-1}$ ). Then, the transferred amount of electron can be calculated as  $1.036 \times 10^{-6}$  mol s<sup>-1</sup> cm<sup>-2</sup> ( $\because F = 96500\text{ C mol}^{-1}\text{ e}^{-}$ ), and H<sub>2</sub> generation rate is calculated as  $5.181 \times 10^{-7}$  mol H<sub>2</sub> s<sup>-1</sup> cm<sup>-2</sup>, which is equivalent to  $3.731 \times 10^{-4}$  g H<sub>2</sub> h<sup>-1</sup> cm<sup>-2</sup>. For producing 1 kg of H<sub>2</sub>, the multiplication constant can be calculated as  $2.681 \times 10^6$  h cm<sup>2</sup>. Since the electrolysis cell operates at 0.169 W cm<sup>-2</sup>, the energy required for producing 1 kg H<sub>2</sub> is calculated as 45.31 kWh. The energy efficiency can be calculated by dividing the theoretical specific energy for 1 kg H<sub>2</sub> production, i.e., 39.4 kWh. Then, the energy efficiency turns out to be 87.0%. Considering the energy efficiency for conventional alkaline electrolysis is less than 70% with the use of platinum electrode, the proposed catalyst can be considered as highly efficient for the water electrolysis.

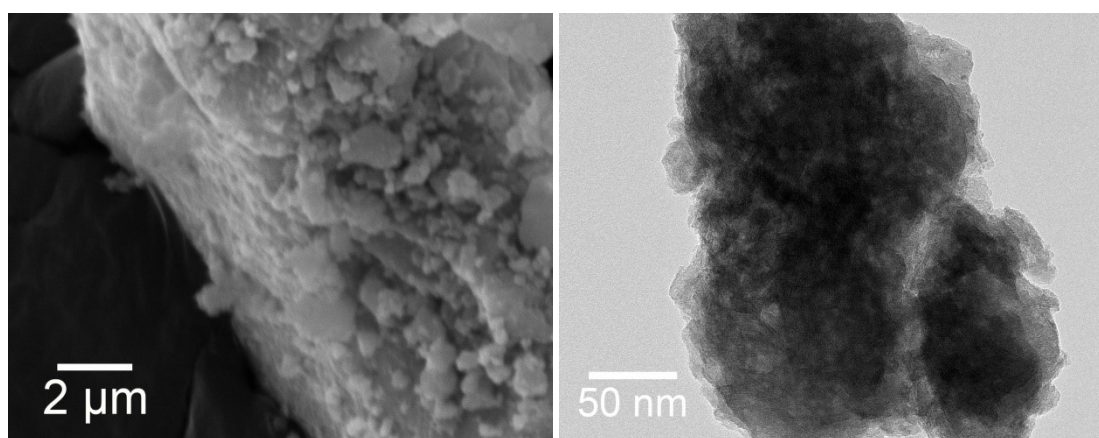


**Fig. S41** (a) SEM image and (b) TEM image of Ni<sub>3</sub>Fe LDH/NiFe<sub>2</sub>O<sub>4</sub>/Pt-Tm after OER testing.

**Table S3** Comparison of OER and HER performances of the as-prepared electrodes with that of other reported LDH-based electrocatalysts evaluated in 1.0 M KOH alkaline solution.

Electrocatalyst	$\eta_{\text{OER}}/\text{mV}$	$\eta_{\text{HER}}/\text{mV}$	Ref.
	(at 10 mA cm <sup>-2</sup> )	(at 10 mA cm <sup>-2</sup> )	
Ni <sub>3</sub> Fe LDH/NiFe <sub>2</sub> O <sub>4</sub> /Pt-Tm	224	125	This work
NiCo-LDH-OH	317	180	<sup>15</sup>
CeCO <sub>3</sub> OH/Ce-CoFe LDH	216	165	<sup>16</sup>
CoMo-LDH	290	115	<sup>17</sup>
NiFe-LDH/FeCoS <sub>2</sub> /CFC	190	308	<sup>18</sup>
CoFeZr/NF	233	159	<sup>19</sup>
H-CoS <sub>x</sub> @NiFe LDH/NF	250	95	<sup>20</sup>
NiCo LDH	227	195	<sup>21</sup>
Pd-NiAl-LDH	264	189	<sup>22</sup>
Mo-CoP	317	118	<sup>23</sup>
Zn <sub>1-x</sub> Fe <sub>x</sub> -oxysele-nide/NF	256	202	<sup>24</sup>
NiFe LDH/NiS <sub>2</sub> /VS <sub>2</sub>	286	76	<sup>25</sup>
Co <sub>0.4</sub> Fe <sub>0.6</sub> LDH/g-CN <sub>x</sub>	280	125	<sup>26</sup>
Co <sub>0.25</sub> Fe <sub>0.75</sub> -LDH	270	365	<sup>27</sup>

## References

1. J. Yu, K. Lu, C. Wang, Z. Wang, C. Fan, G. Bai, G. Wang and F. Yu, *Electrochim. Acta*, 2021, **390**, 138824-138835.
2. K. Bera, R. Madhu, H. N. Dhandapani, S. Nagappan, A. De and S. Kundu, *Inorg. Chem.*, 2022, **61**, 16895-16904.
3. N. Yu, H.-J. Liu, Y.-N. Cao, Q.-Y. Wang, Y. Ma, J.-F. Yu, H. Hu, Y.-M. Chai and B. Dong, *Colloid Surf. A-Physicochem. Eng. Asp.*, 2022, **654**, 130024-130034.
4. J. Yu, Z. Liu, F. Yu, W. Bao, B. Peng, G. Wang, L. Zhang, Y. Xu and F. Wang, *J. Colloid Interface Sci.*, 2022, **623**, 285-293.
5. F. Dionigi, T. Reier, Z. Pawolek, M. Gliech and P. Strasser, *ChemSusChem*, 2016, **9**, 962-972.
6. Z. Chen, M. Ju, M. Sun, L. Jin, R. Cai, Z. Wang, L. Dong, L. Peng, X. Long, B. Huang and S. Yang, *Angew. Chem.-Int. Edit.*, 2021, **60**, 9699-9705.
7. Y. Feng, J. Wei and Y. Ding, *J. Phys. Chem. C*, 2015, **120**, 517-526.
8. H. Xu, C. Shan, X. Wu, M. Sun, B. Huang, Y. Tang and C.-H. Yan, *Energy Environ. Sci.*, 2020, **13**, 2949-2956.
9. Y. Bi, Z. Cai, D. Zhou, Y. Tian, Q. Zhang, Q. Zhang, Y. Kuang, Y. Li, X. Sun and X. Duan, *J. Catal.*, 2018, **358**, 100-107.
10. X. Yin, Y. Hua and Z. Gao, *J. Energy Storage*, 2023, **73**, 109102-109113.
11. Y. Yang, W.-J. Wang, Y.-B. Yang, P.-F. Guo, B. Zhu, K. Wang, W.-T. Wang, Z.-H. He and Z.-T. Liu, *J. Electrochem. Soc.*, 2022, **169**, 024503-024512.
12. S. Zhu, J. Wang, H. Li, J. Cai, Y. Li, J. Hu, Y. He and Y. Zhou, *ACS Appl. Nano*

*Mater.*, 2022, **5**, 13047-13054.

13. A. C. Thenuwara, N. H. Attanayake, J. Yu, J. P. Perdew, E. J. Elzinga, Q. Yan and D. R. Strongin, *J. Phys. Chem. B*, 2017, **122**, 847-854.
14. Z. Chen, Q. Qu, X. Li, K. Srinivas, Y. Chen and M. Zhu, *Molecules*, 2023, **28**, 7289-7302.
15. H. Yang, Z. Zhou, H. Yu, H. Wen, R. Yang, S. Peng, M. Sun and L. Yu, *J. Colloid Interface Sci.*, 2023, **636**, 11-20.
16. J. Tang, J. Hu, X. Chen, B. Yang, K. Zhang, Y. Li, Y. Yao and S. Zhang, *Fuel*, 2024, **365**, 131128-131136.
17. J. Bao, Z. Wang, J. Xie, L. Xu, F. Lei, M. Guan, Y. Huang, Y. Zhao, J. Xia and H. Li, *Inorg. Chem. Front.*, 2018, **5**, 2964-2970.
18. Z. Zhang, J. Zhou, H. Wei, Y. Dai, S. Li, H. Shi and G. Xu, *J. Mater. Sci.*, 2020, **55**, 16625-16640.
19. W. Liu, K. Jiang, Y. Hu, Q. Li, Y. Deng, J. Bao and Y. Lei, *J. Colloid Interface Sci.*, 2021, **604**, 767-775.
20. Y. J. Lee and S.-K. Park, *Small*, 2022, **18**, 2200586-2200596.
21. W. He, D. Cao, D. Ma, Y. Li, C. Chen, L. Liang and H. Liu, *Chem. Commun.*, 2022, **58**, 7757-7760.
22. R. Kalusulingam, M. Mariyaselvakumar, C. A. Antonyraj, S. Mathi, T. S. Mikhailova, S. A. Khubezhov, I. V. Pankov, K. Srinivasan and T. N. Myasoedova, *Energy Fuels*, 2023, **37**, 13319-13330.
23. L. Li, Y. Guo, X. Wang, X. Liu and Y. Lu, *Langmuir*, 2021, **37**, 5986-5992.

24. G. Rajeshkhanna, S. Kandula, K. R. Shrestha, N. H. Kim and J. H. Lee, *Small*, 2018, **14**, 1803638-1803651.
25. T. Wang, X. Zhang, X. Yu, J. Li, K. Wang and J. Niu, *Journal*, 2024, **29**, 951-965.
26. T. Bhowmik, M. K. Kundu and S. Barman, *ACS Appl. Energ. Mater.*, 2018, **1**, 1200-1209.
27. S. Shankar Naik, J. Theerthagiri, F. S. Nogueira, S. J. Lee, A. Min, G.-A. Kim, G. Maia, L. M. C. Pinto and M. Y. Choi, *ACS Catal.*, 2023, **13**, 1477-1491.